A Two-stage Underfrequency Load Shedding Strategy for Microgrid Groups Considering Risk Avoidance

Can Wang [1,*], Zhen Wang [1], Sihu Chu [2], Hui Ma [1], Nan Yang [1], Zhuoli Zhao [4], Chun Sing Lai [3], and Loi Lei Lai[4]

[1] the College of Electrical Engineering and New Energy, China Three Gorges University, Yichang 443002, China
[2] the Hunan Electric Power Design Institute Co., Ltd., China Energy Group, Changsha 410007, China
[3] the Department of Electronic and Electrical Engineering, Brunel University London, London, UB8 3PH, UK
~~[4] the Department of Electrical Engineering, School of Automation, Guangdong University of Technology, Guangzhou, 510006, China~~

Abstract

Underfrequency load shedding is the third level protection measure to ensure the safe and stable operation of power systems, which can effectively prevent the rapid decrease in system frequency caused by power system failure. To compensate for the power deficit resulting from faults during the island operation of a microgrid, a two-stage underfrequency load shedding strategy for microgrid groups considering risk avoidance is proposed in this paper. The proposed strategy divides underfrequency load shedding into a fast load shedding stage and a risk avoidance load shedding strategy. The first stage is fast underfrequency load shedding considering the load frequency characteristics and voltage characteristics; the fast underfrequency load shedding in the first stage reduces the fast frequency decrease before the second stage load shedding operation. The second stage of load shedding is risk avoidance under frequent load shedding. The load shedding in this stage accounts for the risk loss caused by the nondeterminacy of the demand side load to the system load shedding while accounting for the load frequency and voltage characteristics. First, the conditional value at risk (CVaR) theory is introduced in this paper to analyze and determine the risk loss caused by load nondeterminacy on load shedding, and the severity of load shedding (SoLS) is adopted as the CVaR value of load shedding. Second, the underfrequency load shedding optimization model is constructed by taking the risk value of the load shedding conditions of the microgrid as the optimization index of load shedding. Finally, the performance of the proposed strategy is verified based on the improved IEEE-37 node system microgrid group model. The results show that the proposed two-stage load shedding strategy can effectively prevent a rapid decrease in system frequency and effectively reduce the risk loss caused by load nondeterminacy during load shedding.

Keywords: Microgrid groups, Conditional value at risk, Underfrequency load shedding, Load characteristics, Power deficit

* Corresponding author
E-mail address: xfcancan@163.com

1. Introduction

As renewable energy sources develop and popularize, the power industry has entered an era of great change. Distributed power makes the microgrid system active and controllable [1], [2]. Microgrids can form islands to maintain the power supply of important loads when external power grid failures cause power outages [3]. However, the generation uncertainty and intermittency of many distributed energy sources also create problems to the normal running of microgrids [4]. When microgrids cannot satisfy the needs of the load due to the power deficit in the system led by internal or external malfunctions, the frequency of the microgrid will decrease rapidly or even collapse [5]. Power deficit in microgrids seriously threaten the safety and stable operation of microgrids [6], [7]. Underfrequency load shedding (UFLS), as the third level protection measure for the normal running of microgrids, has the function of effectively reducing the system power deficit and ensuring the frequency stability of the power system [8]. Therefore, the design of a logical, effective, and fast underfrequency load shedding strategy has significant research significance for restoring the frequency of microgrids and guaranteeing the secure and normal running of microgrids.

With the development of microgrids, the traditional underfrequency load shedding strategy can no longer meet the needs of today's complex and changeable microgrid operating environment. The development of an adaptive load shedding strategy solves the problem that the traditional underfrequency load shedding strategy is prone to overshedding or undershedding during load shedding [9]. Existing references have conducted extensive research on such load shedding strategies [10]. An adaptive underfrequency load shedding strategy with high permeability for energy storage systems is proposed in [11], which accounts for characteristics such as integrated inertial response and energy storage capacity limitation. A new underfrequency load shedding strategy is proposed in [12] that considers the active power climbing ability of the distributed generation. This strategy takes into account the speed of active power injection in the distributed generation system during load shedding. The above references rely on the high-precision physical model of a microgrid when studying the load shedding strategy, but the adaptability to the disturbance scenario in a microgrid is poor. There are many uncertain factors in microgrid operation, which also influence the normal running of the system. To solve this problem, the Monte Carlo method is used to model the parameter uncertainty problem of the system in the microgrid in [13] and transforms the complex and variable operating environment of the microgrid into a mixed integer linear programming problem. An underfrequency load shedding strategy applicable to the output changes of photovoltaic power stations is proposed in [14], which determines the ratio of load shedding required by each node according to the node voltage stability index. A new centralized adaptive load shedding strategy is proposed in [15], which integrates a load shedding controller and a distribution state estimator to detect the frequency and change rate of the microgrid, so as to determine the load shedding amount. A decentralized adaptive load shedding strategy is proposed in [16], which does not involve the communication link between relays, and separates the continuous frequency threshold in the actual ROCOF function through the voltage drop data to complete the load shedding action. To improve the flexibility of the load shedding strategy, ROCOF is used to calculate the real-time frequency margin in [17], which ensures the execution of the load shedding action. However, the above strategies only consider the disturbance or uncertainty of the power side of the microgrid as the basic foundation to implement the load shedding strategy and take little consideration of the load characteristics of the demand side.

The demand side response, such as the load importance priority, economic loss of the load shedding and risk loss, has a great influence on ensuring the power supply of important loads, quickly recovering the frequency to a stable state, reducing the frequency fluctuation amplitude and reducing the economic loss of the load shedding. Therefore, underfrequency load shedding measures need to reduce the demand-side load in a targeted manner, a load shedding strategy considering load-side load characteristics is proposed. A load shedding strategy applicable to an AC/DC hybrid microgrid is proposed in [18], which constructs the model of load shedding location and load shedding amount by studying the principle of bankruptcy problem, and then realizes the continuous power supply of critical load. The shedding costs of loads of different levels are defined in [19] to minimize the economic losses caused by shedding off important loads. The proposed strategy in [20] considers basic load parameters of multiple load types, such as steady power, steady current, and steady impedance load, when determining the load shedding amount. The above research accounts for the static characteristics of the load when load shedding but does not consider the dynamic characteristics of the load side. Demand-side operation has great uncertainty, which causes unnecessary losses of the system when load shedding strategy is executed.

To describe and reduce the risk of underfrequency load shedding more accurately in microgrids, more accurate assessment methods and models need to be developed, including further analysis and quantitative treatment of risk factors. In this regard, the conditional value at risk (CVaR) method can measure the average loss above a certain risk level, so it can play a very good role in the risk assessment of microgrids. In recent years, the CVAR-based risk assessment method has been applied to power systems. The CVAR-based method is used to solve the optimized dispatching of wind-photovoltaic-energy storage systems with nondeterminacy and demand response in [21], [22]. By using CVaR as a consistency risk measurement, when load shedding is performed, the risk in the process can be corresponded to the decision quantity, and the risk of each load node can be superimposed.

The load shedding strategy increases the calculation time of the load shedding decision when considering load information or system information. To shorten the decision time of the strategy as much as possible, intelligent algorithms and machine learning algorithms to optimize the certainty of the best load shedding location and load shedding capacity have been suggested in the literature [23]. The genetic algorithm is used in [24], [25] to minimize load shedding to reduce load interruption in the system. The particle swarm optimization algorithm is used in [26] to determine the optimal load shedding position of each load shedding step. A hybrid PSO-GA optimization algorithm is proposed in [27], which is used to solve the load shedding objective function to determine the optimal load shedding combination. The above literature combines the intelligent algorithm with the load shedding strategy to enhance the applicability of the load shedding strategy and improve the action speed of the load shedding decision. Priority experience playback and Q-learning are combined in [28] to improve the learning capacity of the controller so that the strategy has a greater ability to adapt to transformation in the running status of microgrid groups. Deep reinforcement learning is used in [29] to adaptively determine the load shedding action, but the focus of the load shedding action is based on voltage stability without considering the system frequency. Although the above strategies based on intelligent algorithms and machine learning algorithms show good potential in adaptive load shedding, the algorithm's generalization is poor in the face of complex and changeable microgrid group operating environments, and reinforcement learning must put a huge number of historical sample and time for training. The operation of underfrequency load shedding needs to be performed quickly and reliably; too much time delay causes the load shedding to be late and causes the system frequency to decline rapidly.

This research figures out the situation of the delay of algorithm decisions and the uncertainty of the load side of microgrid system when load shedding strategy is executed. In this paper, the two-stage load shedding strategy is proposed to compensate for the decision delay problem of the algorithm from the

Table 1
The comparison between the contribution of this paper and the contribution of related literature

Reference	Considering the cost of load shedding	Considering the frequency characteristics	Considering the level of load	Considering the active power-voltage characteristics	Considering the risk loss	Multiple rounds of load shedding	Improving the accuracy of the results
[16]		√		√			√
[17]		√		√		√	√
[19]	√					√	√
[26]		√				√	√
[28]		√	√				√
Proposed strategy	√	√	√	√	√	√	√

strategy, and CVaR theory is used to quantify the load shedding risk caused by load uncertainty. This strategy can not only achieve a lower risk loss cost of load shedding but also make certain the power distribution reliability of significant loads and the frequency stabilization of microgrid system. The main contributions of this paper are as follows, which are different from other methods as shown in Table 1:

- A novel two-stage underfrequency load shedding strategy is proposed to reduce the frequency fluctuation amplitude of microgrids to ensure the stability and reliability of microgrids. It is different from the strategy proposed in [16] using the voltage drop data to separate the continuous frequency threshold in the actual ROCOF function for load shedding; the strategy proposed in [17] using ROCOF for real-time frequency margin calculations to improve the flexibility of the load shedding strategy; and the strategy proposed in [28], which uses algorithm improvement to increase the speed of load shedding action and reduce frequency fluctuations. The proposed strategy reduces the fluctuation amplitude of the system frequency through two-stage load shedding coordination, thus effectively reducing the risks and adverse effects faced by microgrids when the frequency is low.
- To study and determine the risk damage resulting from load uncertainty when load shedding strategy is executed, this paper proposes a quantitative method of load shedding risk loss based on CVaR theory. Different from the load shedding strategy reported in [19] considering the cost and the strategy given in [26] considering the amount of load shedding, in the proposed method, the economic loss of load outage is applied to reflect the loss caused by load shedding of the microgrid, the SoLS risk severity index is defined as the CVaR value of load shedding, and the risk shedding of the system is reduced by removing the load causing large risk loss, simultaneously realizing the minimum risk loss and the optimal load shedding.
- To address the load shedding power distribution problem in the two-stage load shedding strategy, this paper studies the risk degree and frequency fluctuation amplitude, verifies the risk degree and frequency fluctuation amplitude under different load shedding ratios, and finds the optimal load shedding ratio distribution quantity. The optimal load shedding ratio distribution can provide a more scientific and reasonable basis for two-stage load shedding.

2. Problem formulation

The microgrid adopts droop control in island mode, which makes each DG unit operate independently. Using P-f and Q-V droop characteristic curves, when the load power changes, multiple parallel inverter power supplies detect their own output power and reversely fine-tune their own output voltage amplitude and frequency along their own droop curves so that each of them reaches a new stable point and realizes power distribution. When the whole distributed generation of the microgrid can no longer make up for the power deficit by increasing the output power, we must implement the underfrequency load shedding strategy. In this paper, the load shedding and response of distributed generation are combined to calculate the corresponding load shedding value.

If the island power deficit ΔP_{short} detected at the point of common coupling goes beyond the frequency adjustment limit, the microgrid DGs will run by their maximum capacity. Therefore, the load shedding of the microgrid whose frequency is restored to $f^{'}$ after DG regulation is expressed as [30]:

$$\Delta P_{shed}^{total} = \Delta P_{short} - \left(\sum_{i=k+1}^{n} \Delta P_i + \frac{(f_{k+1} - f')}{\Delta f_k} \Delta P_k \right) \tag{1}$$

where ΔP_{shed}^{total} is the total load shedding in the microgrid, ΔP_k is the DG output increment, and Δf_k is the frequency change from frequency f_{k+1} to frequency f_k.

The connection between frequency change and adjustment of active power in equation (1) above is used to determine the total load shedding of the system, and the proposed load shedding plan is executed to shed the relevant load to recover the frequency stability of the microgrid. The load shedding model proposed in this paper is composed of two stages: the first stage of underfrequency load shedding is a fast load shedding model, and the second stage of underfrequency load shedding is a risk avoidance load shedding model. The control timing figure of the designed load shedding strategy is shown in Fig. 1. The specific load shedding steps are as follows:

Step 1: Calculate the total power deficit ΔP_{shed} of microgrid system according to equation (1).

Step 2: According to the load shedding model, assign load shedding $\Delta P_{shed}^{S.1}$ in the first stage and load shedding $\Delta P_{shed}^{S.2}$ in the second stage.

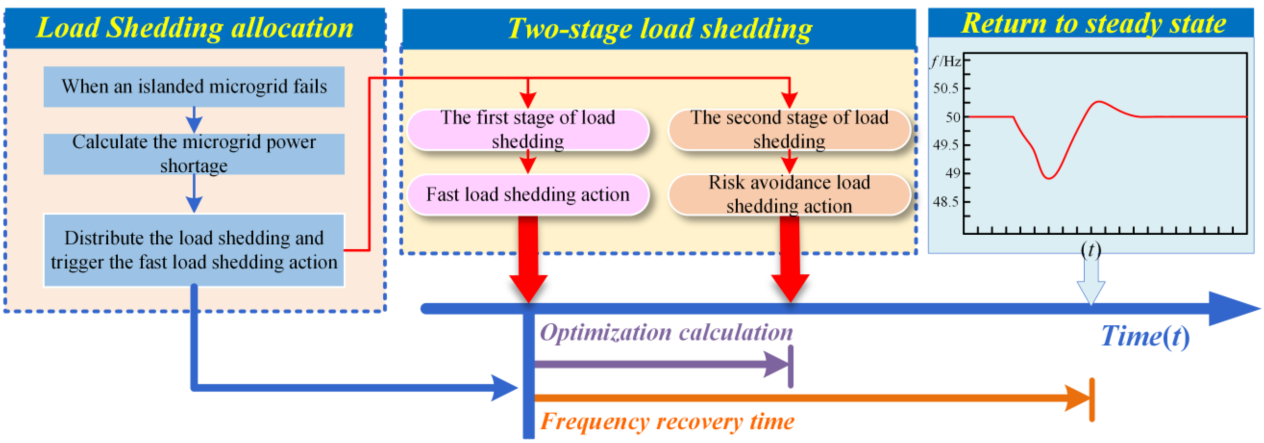

Fig. 1. Control sequence diagram of the proposed load shedding strategy.

Step 3: Implement the first stage of underfrequency load shedding measures to prevent a fast decrease in frequency. At the same time, as the first stage action, the optimal load shedding location and the corresponding load node load shedding amount in the second stage are optimized and solved.

Step 4: After the calculation of the optimal load shedding location and the corresponding node load shedding amount in the second stage is completed, the second stage risk avoidance underfrequency load shedding measures are implemented.

Step 5: Complete all actions of underfrequency load shedding to achieve fast recovery of system frequency.

3. The first stage load shedding model

The first stage load shedding model proposed in this paper is a fast underfrequency load shedding model, which is a rescue strategy to prevent the fast decrease of system frequency when the power deficit takes place in the microgrid system. This stage load shedding action occurs before the second stage load shedding action and is designed to reduce the frequency decrease before the second stage load shedding action. Fast load shedding mainly includes the determination of the load shedding capacity at this stage and the selection of the load shedding location:

3.1. Determination of load shedding

Fast load shedding is used to provide a certain frequency margin for islanded microgrids. Fast load shedding removes a fixed ratio of load $\Delta P_{shed}^{S.1}$ in accordance with the idea of a turn-by-turn scheme. The load shedding in the fast load shedding stage is assigned as $\delta\%$ of the total load shedding, which is expressed as follows:

$$\Delta P_{shed}^{S.1} = \Delta P_{shed}^{total} \times \delta\% \tag{2}$$

where $\Delta P_{shed}^{S.1}$ is the power deficit in the fast load shedding stage, ΔP_{shed}^{total} is the total active power deficiency of the system, and ΔP_{shed}^{total} is calculated by Equation (1).

3.2. Selection of load shedding location

After determining the load shedding capacity for the fast load shedding phase, further determination of the load shedding location for that phase is needed.

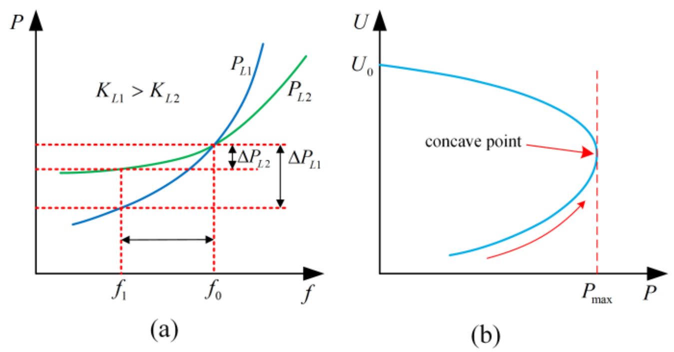

Fig. 2. Load frequency characteristic curve and node P-V.

The effect of frequency regulation is shown in Fig. 2(a). When the system frequency decreases Δf , the active power absorbed from the system by loads with a high frequency regulation coefficient decreases faster. The larger the frequency regulation coefficient K_L of the load, the faster its active power absorption decreases. The load with a small frequency adjustment coefficient K_L is preferentially cut off, while the load with a large K_L is retained. The load frequency adjustment effect can be fully utilized when the frequency declines, thus reducing the active value of the load consumption, which will help to restore the system frequency and cut less load.

Additionally, the active power-voltage characteristics of the load node are referenced, and the P-V curves of the load node cover the weak voltage nodes of the system. Fig. 2(b) shows that as the active power of the transmission line increases, the voltage tends to decrease. The decrease in voltage will reduce the amount of active power load absorption, thus decreasing the frequency damping. P-V curves can provide the index of the sensitivity value dV_i / dP_i, which is expressed as follows:

$$dV_i / dP_i = P_{ti}(V_{ti} - V_{mi}) / V_{ti}(P_{mi} - P_{ti}) \tag{3}$$

where P_{ti} and V_{ti} are the active power and voltage values calculated by the power flow after the disturbances of the previous t times, respectively; P_{mi} and V_{mi} are the active power and voltage values calculated by the power flow after the disturbance near the convex point, respectively. The larger dV_i / dP_i near the convex point indicates that the voltage of the node bus is more sensitive to the change in active power. When the load with larger dV_i / dP_i is removed, the voltage will rise more quickly, and the corresponding load power will be larger. It is unconducive to the frequency recovery. Therefore, under the premise of voltage stability, the node load with small dV_i / dP_i should be cut out preferentially.

In summary, in the fast load shedding stage, the small loads of K_{Li} and dV_i / dP_i are preferentially removed, which helps to alleviate the power imbalance and quickly restore the steady-state frequency. At the same time, load shedding considers the importance of node load, which is classified according to the requirements of power supply reliability and the loss or impact of interruption of the power supply on the economy. It can be divided into level I load, level II load and level III load. Due to different levels of load, their importance is also different. Therefore, when calculating the load shedding disturbance factor, the ratio of its importance weight is different. In this section, load shedding disturbance factor F_{ri} is constructed, which accounts for the importance of node load, frequency regulation effect and active power-voltage characteristics and is expressed as follows:

$$F_{ri} = \lambda_i \cdot (c_1 \cdot \frac{K_{Li}}{\sum_{i=1}^{n} K_{Li}} + c_2 \cdot \frac{dV_i / dP_i}{\sum_{i=1}^{n} dV_i / dP_i}) \tag{4}$$

where F_{ri} is the load shedding disturbance factor of node i; λ_i is the importance weight of node i; c_1 and c_2 are the weight coefficients, and $c_1 + c_2 = 1$ is satisfied; dV_i / dP_i is the sensitivity value of node i; and K_{Li} is the frequency effect adjustment coefficient of node i. n is the total quantity of nodes.

In the first stage, the fast load shedding distribution can be based on the fast load shedding disturbance factor F_{ri} of Equation (4), and nodes with smaller F_{ri} should bear more load shedding. According to the size of F_{ri}, the load shedding capacity of the load node in the fast load shedding stage is allocated as follows:

$$\eta_i = \frac{1}{F_{ri}} (\sum_{i=1}^{n} F_{ri}) \tag{5}$$

$$\varepsilon_i = \frac{\eta_i}{\sum_{i=1}^{n} \eta_i} \tag{6}$$

$$\Delta P_{shed,i}^{S.1} = \varepsilon_i \cdot \Delta P_{shed}^{S.1} \tag{7}$$

$$\sum_{i=1}^{n} \Delta P_{shed,i}^{S.1} = \Delta P_{shed}^{S.1} \tag{8}$$

where η_i represents the inverse parameter of disturbance factor F_{ri} of node i; F_{ri} is the disturbance factor of node i; ε_i is the ratio of inverse ratio parameter η_i; $\Delta P_{shed,i}^{S.1}$ is the load shedding assigned in the fast load shedding phase of node i; and $\Delta P_{shed}^{S.1}$ is the total load shedding capacity in the fast load shedding stage.

4. The second stage load shedding model

The second stage underfrequency load shedding model is a risk avoidance load shedding model. Risk avoidance load shedding is a load shedding measure to make up for the residual power deficit of the system after fast load shedding. At this stage, the system frequency will be greatly adjusted, and the load will be selectively removed. This section introduces conditional value at risk (CVaR) to quantify the risk of load uncertainty loss $F_{SoLS,i}$ caused by load shedding in microgrid systems. CVaR can be used to effectively predict and assess the extent of losses caused by uncertain events [31]. The normal running of the microgrid is the result of load power and generator output coordination, and the essential cause of risk is the rated power deviation caused by uncertain factors. The power fluctuation on the load side, the error of measurement and the inaccuracy of prediction are all uncertain events, and the use of CVaR can better reflect the potential risk loss caused by load power uncertainty during load shedding of an islanded microgrid. The risk-averse load shedding model established in this stage is designed to minimize the risk loss of load shedding, minimize the system disturbance factor, and reduce the risk loss caused by load uncertainty when the load shedding strategy is implemented.

4.1. Determination of load shedding

The load shedding in the risk avoidance phase occurs after the fast load shedding, and the load shedding amount is the total power deficit at the time of island occurrence minus the power deficit in the fast load shedding stage, expressed as follows:

$$\Delta P_{shed}^{S.2} = \Delta P_{shed}^{total} - \Delta P_{shed}^{S.1} \tag{9}$$

4.2. Selection of load shedding location

This stage of risk avoidance load shedding mainly considers the load risk loss in the process of system load shedding. When reducing the load, priority should be given to removing the loads with a low-risk loss of load shedding during the microgrid and in the meantime removing the loads with a small disturbance factor. To construct the load shedding risk loss degree factor F_{SoLS}, the objective function of load shedding optimization at this stage is as follows:

$$\min \sum_{i=1}^{n} (\varphi_1 F_{SoLS,i} + \varphi_2 F_{ri}) \tag{10}$$

where φ_1 and φ_2 are the weight coefficients and satisfy $\varphi_1 + \varphi_2 = 1$; $F_{SoLS,i}$ is the degree of risk of loss of the i load; and F_{ri} is the load shedding perturbation factor.

The fluctuation of the active power of the node load is an important uncertainty factor faced by microgrids. In this research, the load power adopts the normal distribution model [32]. Assuming that the active power of the load node i satisfies the normal distribution, the normal distribution model and probability density function of the load power are as follows:

$$P_{Li} \sim N(\mu_i, \sigma_i^2) \tag{11}$$

$$\rho(\xi) = \frac{1}{\sigma\sqrt{2\pi}} e^{-\frac{(\xi-\mu)^2}{2\sigma^2}} \tag{12}$$

where P_{Li} is the load active power of node i; μ_i and σ_i^2 are the expected and variance of the load active power of node i, respectively; μ_i is the mean load power $P_{LN,i}$ of node i; and σ_i^2 is 10% of the expected power.

For a given confidence level $\beta \in (0,1)$, the corresponding VaR and CVaR are obtained from the following equation [33]:

$$\psi(x,\alpha) = \int_{f(\xi,x)\le\alpha} \rho(\xi) d\xi \tag{13}$$

$$F_{VaR} = \alpha_\beta(x) = \min\left\{\alpha \in R : \psi(x,\alpha) \ge \beta\right\} \tag{14}$$

$$F_{CVaR} = \frac{1}{1-\beta} \int_{f(\xi,x)\ge\alpha_\beta(x)} f(\xi,x)\rho(\xi) d\xi \tag{15}$$

where $\rho(\xi)$ is the probability density function of the random variable ξ that determines the risk loss of the system; $f(\xi,x)$ is the system risk loss function caused by the combination of decision variables x and random variables ξ; $\psi(x,\alpha)$ is a distribution function whose risk loss is not greater than the boundary value α; and F_{VaR} and F_{CVaR} are the value-at-risk cost VaR and conditional value-at-risk cost CVaR under confidence level β.

Since an analytical expression for $\alpha_\beta(x)$ is difficult to obtain directly, the auxiliary function is introduced:

$$F_{CVaR} = F(x,\alpha) = \alpha + \frac{1}{1-\beta} \int_{\xi\in R} \left[f(\xi,x) - \alpha\right]^+ \rho(\xi) d\xi \tag{16}$$

$$\left[f(\xi,x) - \alpha\right]^+ = \max\left\{f(\xi,x) - \alpha, 0\right\} \tag{17}$$

The risk loss function $f(\xi,x)$ can be expressed by the economic loss of user outages, and the risk economic loss caused by load shedding is expressed as follows:

$$M_{LOSS} = \sum_{i=1}^{n} M_{loss,Li} = \sum_{i=1}^{n} C_{loss,i} P_{loss,Li}, \quad P_{loss,Li} \geq 0 \tag{18}$$

$$P_{loss,Li} = \omega_i \cdot P_{Li} \tag{19}$$

where M_{LOSS} is the total economic loss of the load shedding; $M_{loss,Li}$ is the economic loss for the removal of load i; $C_{loss,i}$ is the load i removal loss factor, which represents the economic loss caused by the loss of unit power of load i; $P_{loss,Li}$ is the load i amount of load shedding; ω_i is the load shedding ratio coefficient of load i; P_{Li} is the active power for the load of node i; and n is the total number of load nodes.

Assessment of the severity of the risk of load shedding can help the system identify and address potential risks in a timely manner, thereby ensuring the reliability and stability of the system. To quantitatively assess the severity of load shedding risk, this paper defines the severity indicator of load shedding risk SoLS as the CVaR value of load shedding. Under a certain confidence level, the average underlying economic loss suffered by the system when the economic loss of the load i outage exceeds the VaR critical value over a future period is expressed as:

$$F_{SoLS} = \alpha + \frac{1}{(1-\beta)n} \sum_{i=1}^{n} [C_{loss,i} \cdot \omega_i \cdot P_{Li} - \alpha]^{+} \tag{20}$$

However, the risk degree of the load shedding loss of a single load is calculated as follows:

$$F_{SoLS,i} = \frac{\alpha}{n} + \frac{1}{(1-\beta)n} [C_{loss,i} \cdot \omega_i \cdot P_{Li} - \alpha]^{+} \tag{21}$$

where F_{SoLS} is the risk degree of load shedding loss; $F_{SoLS,i}$ is the risk degree of the load shedding loss of node i; α is the limited value; and β is the confidence level; n is the total number of load nodes.

To make the underfrequency load shedding meet the system control requirements, the following constraints should be met:

$$\begin{cases} P_i(t) - U_i(t) \sum_{j \in i} U_j(t) (G_{ij} \cos\theta_{ij}(t) + B_{ij} \sin\theta_{ij}(t)) = 0 \\ Q_i(t) - U_i(t) \sum_{j \in i} U_j(t) (G_{ij} \cos\theta_{ij}(t) - B_{ij} \sin\theta_{ij}(t)) = 0 \end{cases} \tag{22}$$

$$f_{\min} \leq f \leq f_{\max} \tag{23}$$

$$P_{loss,Li} \leq P_{loss\max,Li} \tag{24}$$

$$\sum_{i=1}^{n} P_{loss,i} = \Delta P_{shed}^{S.2} \tag{25}$$

where $P_i(t)$ and $Q_i(t)$ are the active power and reactive power of the t time for node i, respectively; $U_i(t)$ and $U_j(t)$ are the voltage amplitude of node i and node j, respectively; $\theta_{ij}(t)$ is the i and j phase difference between nodes; and G_{ij} and B_{ij} are the conductance and susceptance between nodes i and j, respectively. f represents the frequency of the bus; $f_{\min}$ and $f_{\max}$ indicate the maximum and minimum bus frequency values, respectively; $P_{loss\max,Li}$ is the maximum load shedding power of the i load; and $\Delta P_{shed}^{S.2}$ is the total amount of load shedding for the second stage.

The loss risk index of the load i is taken as the main factor for the second stage load shedding into Equation (10), and then the grasshopper optimization algorithm (GOA) is applied to calculate the load shedding objective function to get the second stage optimal load shedding strategy.

5. Case study

5.1. Microgrid group model

To verify the effectiveness of the underfrequency load shedding strategy proposed in this paper, the microgrid group model based on the improved IEEE-37 node system is built in MATLAB/Simulink, as shown in Fig. 3 [34]. Table 2 shows the configuration information of the microgrid group, which includes three submicrogrids MG1, MG2 and MG3. The MG1 submicrogrid contains three photovoltaic modules PV1-3, one energy storage module BES1, and three loads LD1-3. The MG2 submicrogrid contains three photovoltaic modules PV4-6, three energy storage modules BES2-4, and four loads LD4-7. The MG3

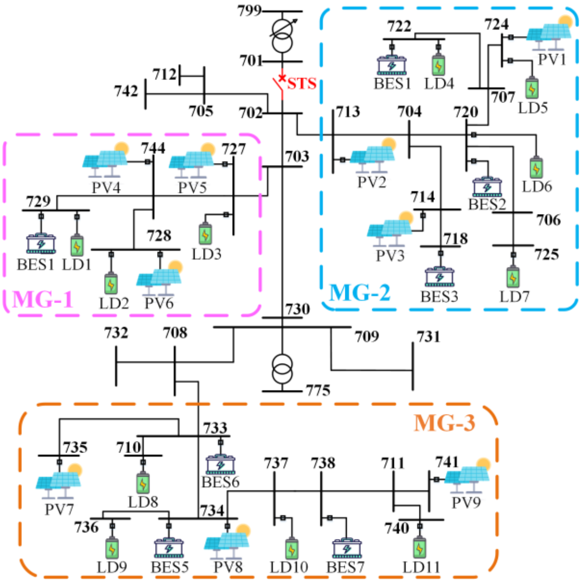

Fig. 3. Microgrid group model based on the improved IEEE37 node system.

Table 2
Microgrid group configuration information

Microgrid	MG-1	MG-2	MG-3
	PV1-3	PV4-6	PV7-9
Rated photovoltaic (PV) power (kW)	50,50,50	70,70,70	60,60,60
PV real-time power (kW)	30,30,30	40,40,40	40,40,40
	BES1	BES2-4	BES5-7
Rated power of BES (kW)	300	90,70,60	100,70,80
BES real-time power (kW)	200	70,40,30	80,40,50

Table 3
System load data information

Bus	Level	$P_{LN,i}$ kW	$P_{loss\max,Li}$ kW	$C_{loss,i}$ ($/kWh)	σ_i^2
LD1	III	100	70	0.42	10
LD2	I	60	30	3.05	6
LD3	II	95	52	1.76	9.5
LD4	III	50	35	1.69	5
LD5	II	75	33	1.24	7.5
LD6	I	55	20	2.05	5.5
LD7	II	55	20	0.79	5.5
LD8	III	110	65	0.96	11
LD9	I	80	45	1.01	8
LD10	III	84	64	0.84	8.4
LD11	II	76	50	1.35	7.6

submicrogrid contains three photovoltaic modules PV7-9, three energy storage modules BES5-7, and four loads LD8-11. Table 3 shows the data information of the 11 load nodes of the system. They are classified into Level I loads, Level II loads, and Level III loads in decreasing order of level.

5.2. Case A: two-stage load shedding allocation verification

This section mainly tests the impact of the allocation of different ratios of the proposed load shedding strategy on the frequency fluctuation and the loss of the load shedding risk. The island switching time is set to t =0.5 s, and the actual output power of BES1 is 20% of the original value due to the fault during the island switching of the microgrid group, which is 40 kW. In this scenario, the microgrid group in islanded operation mode can no longer reach the power requirement of the full load, and a portion of the load must be removed to allow the system to run in a normal and stable condition. The communication network in this paper is shown in Fig. 4. The improved IEEE-37 node microgrid group model is equipped

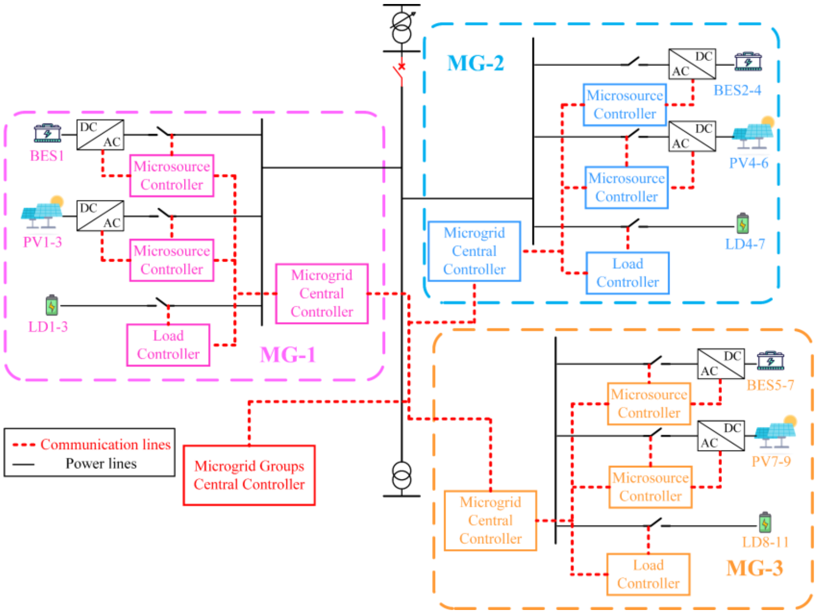

Fig. 4. Communication network of the microgrid group based on the improved IEEE-37 node system.

with a Microgrid Groups Central Controller, which is responsible for transmitting signals to each Microgrid Central Controller. The Microgrid Central Controllers are set up in MG1, MG2 and MG3 respectively, which are responsible for receiving instructions from the Microgrid Group Central Controller and transmitting instructions to the Load Controller and Microsource Controller. The microgrid in China adopts optical fiber communication technology and a Modbus communication protocol (GB/T 36270-2018). Considering the transmission refractive index, the actual transmission rate of the fiber is approximately 200,000 kilometers per second. Therefore, when implementing the underfrequency load shedding strategy, the communication transmission delay is set to 10 ms, and the relay startup and underfrequency load shedding delay is set to 10 ms [35]. Based on Equation (1), the load shedding in this island scenario is calculated to be 169 kW.

The distribution of the first load shedding ratio in the two-stage load shedding affects the uncertainty risk of load shedding in the second load shedding. Too much shedding amount in the first stage will make the risk of load uncertainty in the second stage of load shedding insufficiently considered, which will cause greater loss, but too little load shedding amount cannot effectively reduce the rapid decrease in frequency. To this end, this section will test and verify the two-stage load shedding allocation to find a suitable load shedding allocation ratio, so as to minimize the amplitude of frequency variation caused by the load shedding and the risk loss caused by the system load shedding.

In this paper, the frequency recovery effect of different ratio allocations of two-stage load shedding on multimicrogrid island operation is tested, as shown in Fig. 5. The test results show that when the load

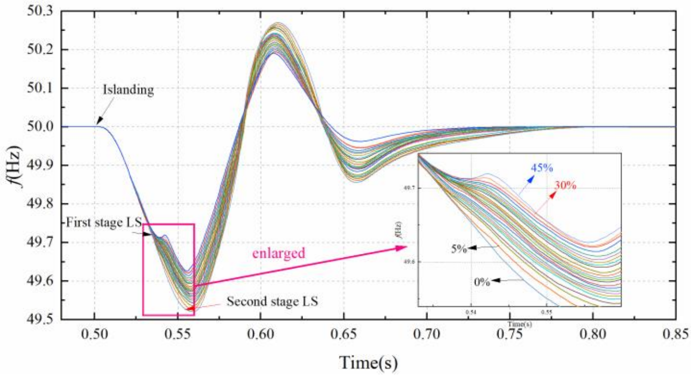

Fig. 5. Comparison chart of frequency recovery for different load shedding allocation ratios.

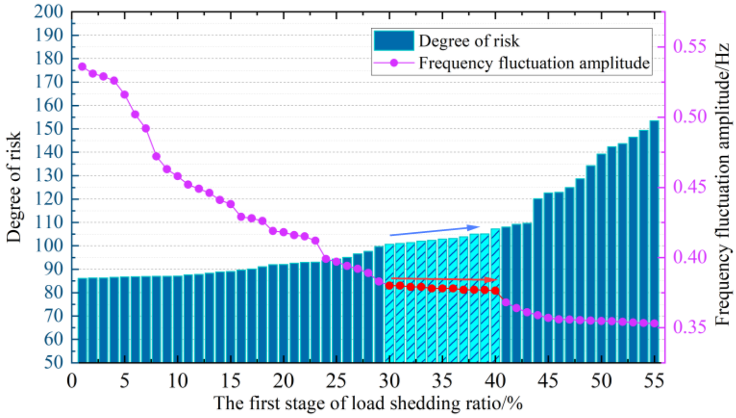

Fig. 6. Comparison chart of the risk loss degree and frequency fluctuation range under different load shedding ratios.

shedding ratio of the first stage is 0~10%, the suppression effect of the first stage load shedding on the frequency decrease is not obvious. As the ratio of the first stage load shedding increases, the frequency decrease amplitude decreases after the first load shedding. When t=0.558 s, based on the second stage of CVaR load shedding, the frequency is greatly adjusted. Since the first stage of load shedding has a certain frequency adjustment effect, the frequency fluctuation amplitude during the second stage of load shedding is significantly smaller than that without the first stage of load shedding (0%). The test results show that the proposed first-stage load shedding measure can effectively suppress the fast frequency decrease before the second-stage load shedding action. Different load shedding ratios produce different frequency suppression effects, and further testing is required to select the appropriate allocation ratio of load shedding.

Fig. 6 is a comparative chart of load risk severity indicators and frequency fluctuation amplitudes under different load shedding ratios in the first stage. In Fig. 6, the change trend shows that when the load shedding ratio of the first stage increases, the degree of load risk loss of the system also increases correspondingly, and the frequency fluctuation range of the system decreases. Because the first stage of load shedding is based on the fast load shedding action which is affected by the load frequency and P-V characteristics, the risk caused by the uncertainty of the load power and the loss of load shedding are not considered. Therefore, the degree of load risk loss increases with the increase in the ratio of load shedding in the first stage. The first stage inhibits the frequency decrease, and the frequency fluctuation amplitude of the system will be reduced as the load shedding ratio of the first stage increases. From Fig. 6, when the load shedding ratio in the first stage exceeds 30% and is at 30%~40%, the reduction effect of the frequency fluctuation amplitude in this stage is relatively flat, and the increase in the degree of system risk loss at this stage is also relatively flat. Comprehensively considering the frequency fluctuation range and the degree of load risk loss, within making certain that the frequency fluctuation range of microgrid system is small and the degree of risk loss is not large, this paper sets the load shedding ratio of the first stage to be 30% of the power deficit.

5.3. Case B: the impact of different risk appetites on load shedding actions

According to the analysis result of Case A, this paper sets the load shedding amount of the first stage to be 30% of the total load shedding. In this island switching scenario, the influence analysis of different confidence levels on load shedding actions is discussed; at the same time, the change in the risk degree is analyzed. The confidence level is changed, and the value of β is increased from 0.9 to 0.99 in steps of 0.01. Based on CVaR, the degree of risk of load shedding loss F_{SoLS} and load shedding under different confidence levels are calculated as shown in Fig. 7. The results show that with the improvement of confidence level β, the security requirements of microgrids increase, and the risk loss and load shedding of microgrids in island mode also increase. As the confidence level increases, the system becomes more sensitive to the risk loss caused by load power uncertainty. When β approaches 0.9, the proposed strategy has a small degree of risk loss and has a small load shedding of 159.8 kW. When β approaches

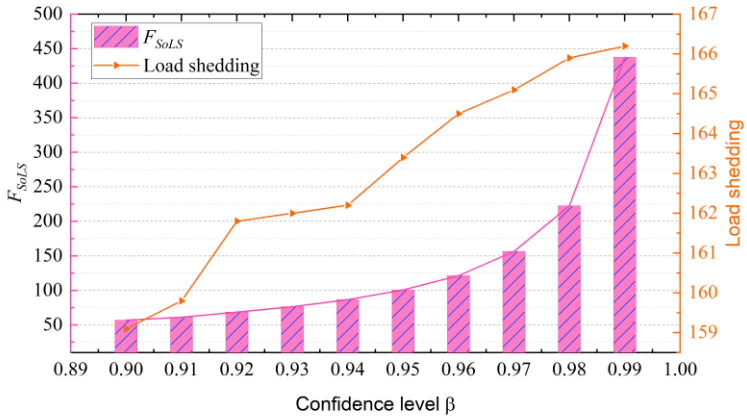

Fig. 7. Comparison chart of risk loss and load shedding at different confidence levels.

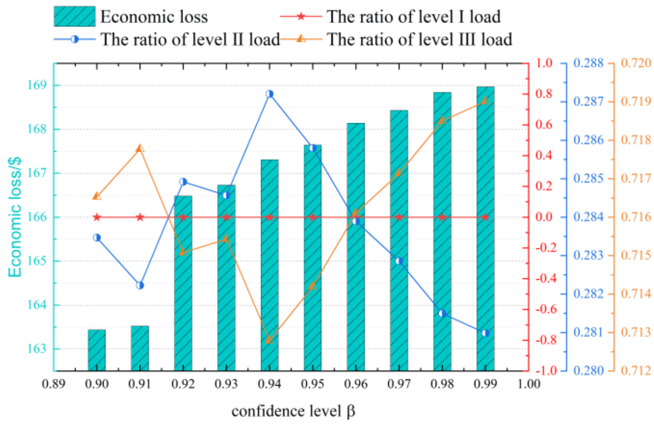

Fig. 8. Economic loss at different confidence levels and the ratio of loads removed at each level.

0.99, the risk loss caused by microgrid load shedding is the largest, reaching \$437.62. In the confidence range of the test, the maximum load shedding is 166.2 kW when the confidence level is 0.99, which indicates that the system cuts off more loads to guarantee the normal running of microgrid system to avoid the risk caused by the uncertainty of load power. Although the load shedding in this time is greater than that at other confidence levels, the load shedding of 166.2 kW in this time is still less than the calculated value of 169 kW for power deficit. The test results also show that the strategy proposed in this paper can reduce the amount of load shedding and ensure a greater load power supply in microgrid system.

The economic loss of load shedding and the ratio of load shedding in each level within the confidence range [0.9, 0.99] are shown in Fig. 8. When the confidence level β increases from 0.9 to 0.99, the economic loss of load shedding also increases by 3.38% because with the increase in confidence level, the risk sensitivity caused by load uncertainty increases, which in turn leads to worse economy of microgrid system. Meanwhile, from the ratio of each load type of load shedding, the strategy proposed in this paper avoids the resection of level I load when resecting the load under different confidence levels. The above analysis proves that the proposed strategy can guarantee the dependable power supply of level I loads in the microgrid.

5.4. Case C: comparative analysis of underfrequency load shedding strategies

This section compares and analyzes the difference between the load shedding performance of the proposed strategy and other load shedding strategies in the island operation mode. The confidence level $\beta = 0.95$ is regarded as an example to verify the effects of the proposed strategy. In the case of an island, the proposed load shedding Strategy A, the adaptive load shedding Strategy B considering the load shedding cost [19], the load shedding Strategy C using the PSO optimization algorithm [26], the load shedding strategy D using DQN [28], the decentralized underfrequency load shedding strategy E based on the voltage drop data setting frequency threshold [16] and the underfrequency load shedding strategy F based on the ROCOF estimation frequency stability margin [17] are used for the load shedding test and comparative analysis. The six underfrequency load shedding strategies of A, B, C, D, E and F are executed. The ratio of load shedding nodes in each load shedding strategy is shown in Fig 9. The node ratio of Strategy B load shedding is shown in Fig. 9(b), and Strategy B mainly considers the removal cost of different loads when load shedding and tries to avoid excessive economic losses when selecting the load shedding. However, this strategy does not consider the power supply of important loads, resulting in the removal of LD9 of the important load accounting for 2.74% of the total load shedding. The ratio of load shedding nodes in strategy C is shown in Fig. 9(c), which considers the system frequency response and load shedding constraints without paying attention to the level of the load when the load shedding strategy is executed. It removes the level I load LD2,6,9 during load shedding, accounting for 11.64% of the total load shedding. The node ratio of Strategy E load shedding is shown in Fig. 9(e). This strategy considers the frequency characteristics and active power-voltage characteristics of the system without considering the level of the load when the load shedding strategy is executed. Therefore, it removes the level I load LD2,6,9 during load shedding, accounting for 10.62% of the total load shedding. The node ratio of Strategy F load shedding is shown in Fig. 9(f). This strategy is mainly based on the flexibility of load shedding when the load shedding strategy is executed, considering the frequency stability margin, but does not consider the level of load, so that the removal of the level I load LD6 and 9 accounts for 5.78% of the total load shedding. Figs. 9(a) and (d) show the ratio of excision load types in Strategies A and D, respectively, and both strategies avoid the shedding of important loads under the premise of considering the level of loads. However, Strategy A considers the level of the load, the frequency characteristics of the load, the P-V characteristics, and other aspects. By considering these factors comprehensively, it is possible to judge the importance of the current load more accurately and avoid misjudgment. In contrast, Strategy D only treats the level of the load as a single load attribute and cannot finely distinguish the level of the load, so it may lead to the risk of removing some of the important loads. In summary, compared with strategies B, C, D, E and F, strategy A ensures the power supply of the level I load during load shedding and has better power supply reliability.

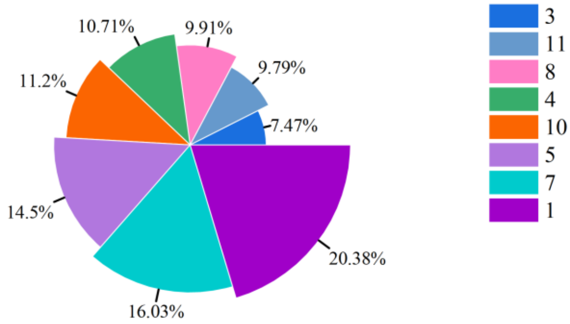
10.71%
9.91%
9.79%
11.2%
7.47%
14.5%
20.38%
16.03%
3
11
8
4
10
5
7
1

(a)

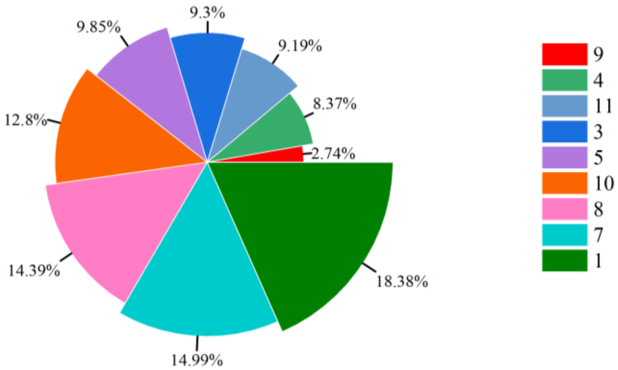
9.3%
9.85%
9.19%
8.37%
12.8%
2.74%
14.39%
18.38%
14.99%
9
4
11
3
5
10
8
7
1

(b)

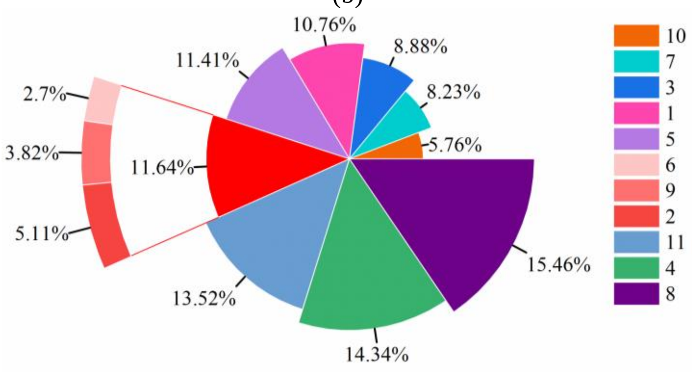
10.76%
11.41%
8.88%
8.23%
2.7%
5.76%
3.82%
11.64%
5.11%
15.46%
13.52%
14.34%
10
7
3
1
5
6
9
2
11
4
8

(c)

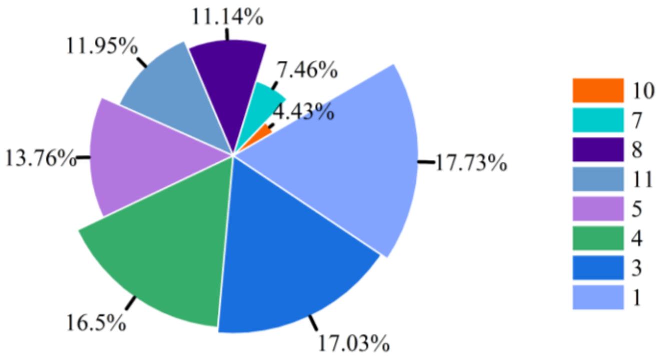

(d)

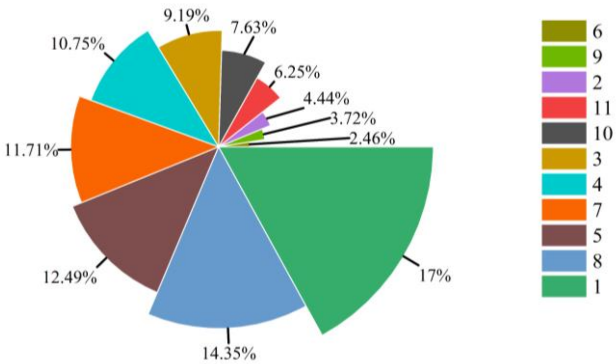

(e)

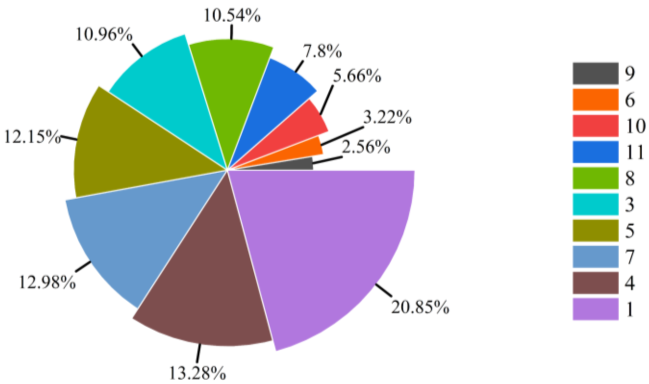

(f)

Fig. 9. The ratio of load shedding nodes in the total load shedding of Case C.

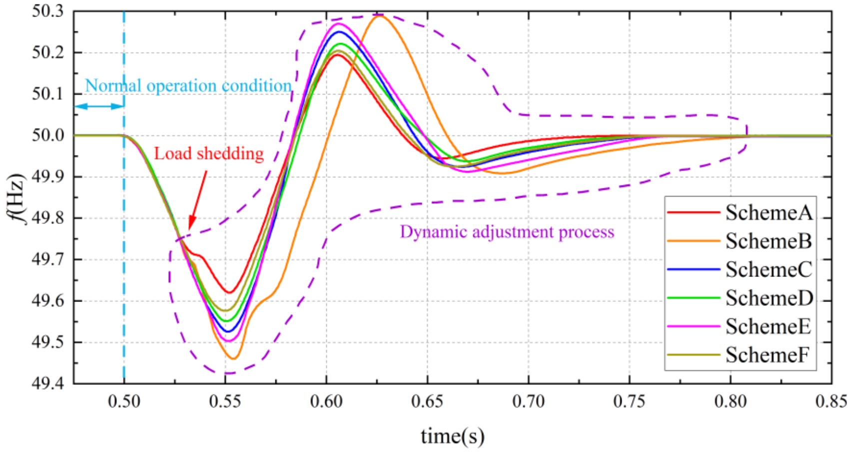

Fig. 10. Frequency fluctuation comparison chart for Case C.

Table 4

Comparison information of underfrequency load shedding strategies

	Strategy A	Strategy B	Strategy C	Strategy D	Strategy E	Strategy F
$C_{\cos t}$ /$	167.643	181.439	217.674	203.758	204.617	186.774
t_{rec} /s	0.2344	0.2896	0.2672	0.2568	0.2688	0.2614
Δf /Hz	0.38	0.5395	0.4747	0.4484	0.4927	0.4257
P_{LS} /kW	163.4	178.8	170.1	171.5	172.9	171.4

The waveform diagram of frequency recovery after load shedding action is shown in Fig. 10, and the load economic loss $C_{\cos t}$, frequency recovery time t_{rec}, frequency fluctuation amplitude Δf and load shedding amount P_{LS} after load shedding action of each strategy are shown in Table 4. Among them, the total economic loss of load shedding is the total economic loss of the load removed in two stages. Compared with Strategies B, C, D, E and F, the proposed Strategy A has 7.6%, 22.98%, 17.72%, 18.07% and 10.24% less economic losses in load shedding, respectively. Because Strategy B is implemented with the economy of load in mind and Strategies C, D, E and F do not consider this factor in load shedding, Strategy B causes smaller economic losses of load than Strategies C, D, E and F. However, Strategy A accounts for the uncertainty of the load based on CVaR and evaluates the risk loss degree of load shedding when the load is removed so that the economic risk loss caused by the resected load is minimized. In terms of the frequency recovery effect, the frequency fluctuation range caused by Strategy A is 0.38 Hz, which is 29.56%, 19.95%, 15.25%, 22.87% and 10.74% smaller than that of Strategies B, C, D, E and F, respectively. Because strategy F uses ROCOF to estimate the frequency stability margin, it ensures the flexibility of the load shedding strategy, while strategies B, C, D and E do not involve this aspect during load shedding, so the frequency fluctuation of strategy F is smaller than that of strategies B, C, D and E. When the system power deficit is calculated, the first and second stages of load shedding Strategy A are allocated, and the first stage load shedding action is directly implemented based on the load characteristics and voltage characteristics. During the first stage of load shedding, the second stage of load shedding is simultaneously solved by the optimal load shedding scheme. Since the fast load shedding of the first stage prevents the fast decrease of the frequency before the action of the second stage, the fluctuation amplitude of the frequency can be effectively reduced. The frequency recovery time is 19.06%, 12.28%, 8.72%, 12.8% and 10.33% less than that of Strategies B, C, D, E and F, respectively. The proposed Strategies B and C have a delay in optimization solving and require waiting time response for load shedding decisions, so their decision speed is slower than that of Strategy A, resulting in a worse time recovery effect. Although strategy E is decentralized load shedding that does not depend on the communication network, to ensure the frequency recovery effect, it is necessary to set a time delay between continuous load shedding stages. Strategy F provides flexibility for load shedding by estimating the frequency stability margin, but it increases the time delay of the action to a certain extent, resulting in slow frequency recovery. The load shedding decision of Strategy D based on the DQN algorithm is faster than the second stage of Strategy A, but the first stage load shedding of Strategy A can perform fast load shedding action before the second stage of load shedding, and its action occurs before the DQN decision, so Strategy A has a faster recovery effect. From the load shedding of each strategy in Table 4, the proposed Strategy A has the smallest load shedding amount and Strategy B has the largest load shedding. Since Strategy A fully considers the frequency regulation effect of the load in load shedding, this effect helps to restore the frequency of the system and remove less load. Strategies B, C, D, E and F do not consider this feature, and strategies B, C and F all adopt multiple rounds of load shedding. Based on this multiround load shedding strategy, the phenomenon of overshedding occurs, and the load shedding of Strategies B and C exceeds the power deficit of 169 kW in the island scenario. Strategy D does not take into account the corresponding time delay and measurement error when calculating the load shedding so that the load shedding amount during load shedding also exceeds the total calculated power deficit. Both Strategy E and Strategy F adopt the ROCOF relay, but the measurement error is not considered, so that the phenomenon of overshedding also occurs.

Through the Case C test analysis, the proposed Strategy A can take into account both the uncertainty of the load and the frequency regulation effect as considering the uncertainty of the load based on CVaR, which can effectively decrease the economic loss and frequency fluctuation range of the microgrid system. The cooperation of the proposed two-stage load shedding strategy can effectively improve the speed of frequency recovery, minimize the amount of load shedding, and have better underfrequency load shedding performance. Although Strategies B, C, D, E and F each adopt different optimization and control methods, they lead to large economic losses, frequency fluctuations in load shedding decisions, and a slow speed of frequency recovery. Therefore, the proposed Strategy A has a better underfrequency load shedding effect, which is conducive to improving frequency stability and economy in islanded microgrids.

6. Conclusion and results

To address the problem of fast frequency decrease in islanded microgrids and the economic loss caused by load power uncertainty, this paper proposes a two-stage load shedding strategy based on load risk avoidance. The proposed strategy is composed of two stages. The first stage uses the fast load shedding action to reduce the frequency of fast decrease caused by the delay of the strategy action caused by the algorithm before the risk avoidance load shedding action in the second stage. The second stage considers the uncertainty of load power based on CVaR theory and quantifies the degree of risk loss caused by load power fluctuation uncertainty to load shedding. Through the two different stages of load shedding strategies, the load is evaluated, and the corresponding load is removed so that the system recovery frequency is stable, and the cooperation between strategies is used to complete fast and reliable load shedding to prevent a fast decrease in frequency. The research results demonstrate that contrasted with the general adaptive load shedding strategy, the adaptive load shedding strategy using the intelligent algorithm and the adaptive load shedding strategy using the DQN algorithm, the strategy proposed in this paper can be used to effectively reduce the fluctuation amplitude of the frequency of the islanded microgrid and reduce the frequency recovery time. In addition, the proposed strategy can be used to effectively reduce the system economic risk loss caused by load power uncertainty and realize the double improvement of operation reliability and economy in the islanded state of the microgrid.

Declaration of Competing Interest

The authors declare that they have no known competing financial interests or personal relationships that could have appeared to influence the work reported in this paper.

Acknowledgements

This work was supported in part by the National Natural Science Foundation of China under Grant 52107108, and in part by the Natural Science Foundation of Hubei Province under Grant 2021CFB163.

Appendix A

To analyze whether the first stage load shedding ratio share under different networks is universal, a microgrid group model based on the improved IEEE-33 node system is built in MATLAB/Simulink, as shown in Fig. A1. Table A1 shows the configuration information of the microgrid group, which includes three submicrogrids MG1, MG2 and MG3. The MG1 submicrogrid contains three photovoltaic modules

Table A1

Microgrid group configuration information (improved IEEE-33 node system)

Microgrid	MG1	MG2	MG3
	PV1-3	PV4-6	PV7-9
Rated photovoltaic(PV) power(kW)	50,50,50	50,50,50	50,50,50
PV real-time power(kW)	30,30,30	30,30,30	30,30,30
	BES1	BES2-4	BES5-7
Rated power of BES(kW)	150	80,50,40	70,70,50
BES real-time power(kW)	130	60,30,20	50,50,30

Table A2

System load data information (improved IEEE-33 node system)

Bus	Priority	$P_{LN,i}$ kW	$P_{loss,\max,Li}$ kW	$C_{loss,i}$ ($/kWh)	σ_i^2
LD1	II	80	35	1.67	8
LD2	I	60	30	3.05	6
LD3	III	50	20	0.78	5
LD4	III	70	50	0.97	7
LD5	II	50	22	1.21	5
LD6	I	60	35	2.53	6
LD7	I	40	32	1.43	4
LD8	III	60	40	1.23	6
LD9	II	90	65	1.72	9

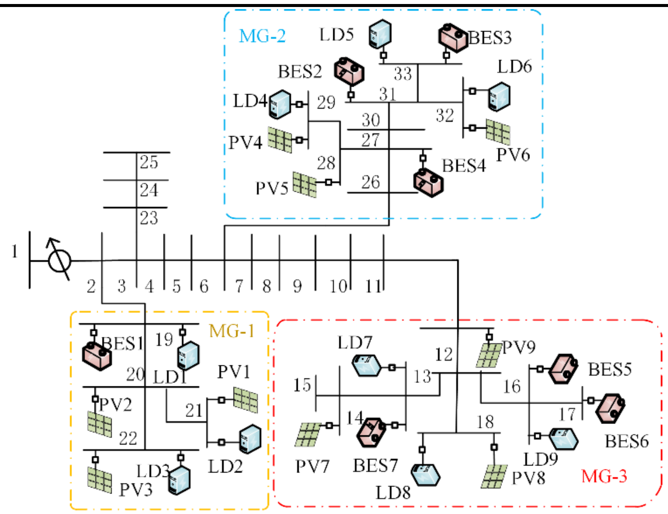

Fig. A1. Microgrid group model based on the improved IEEE-33 node system.

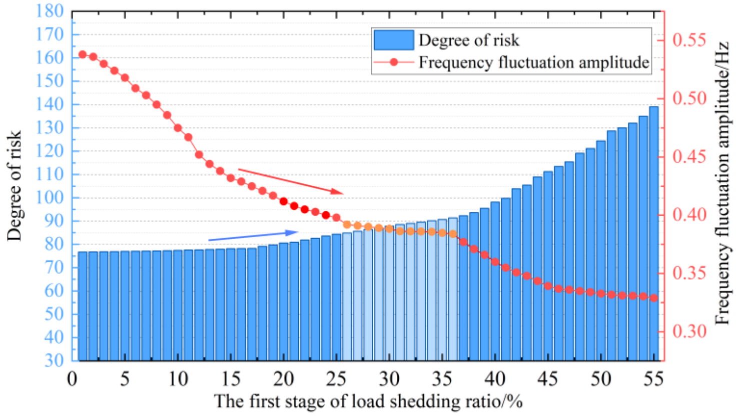

Fig. A2. Comparison chart of the risk loss degree and frequency fluctuation range under different load shedding ratios (improved IEEE-33 node system).

PV1-3, one energy storage module BES1, and three loads LD1-3. The MG2 submicrogrid contains three photovoltaic modules PV4-6, three energy storage modules BES2-4, and three loads LD4-6. The MG3 submicrogrid contains three photovoltaic modules PV7-9, three energy storage modules BES5-7, and three loads LD7-9. Table A2 shows the data information of the 9 load nodes of the system. They are classified into Level I loads, Level II loads, and Level III loads in decreasing order of level.

Fig. A2 is a comparative chart of the load risk severity indicators and frequency fluctuation amplitudes under the different load shedding ratios in the first stage (improved IEEE-33 node system). With the increase in the ratio of load shedding in the first stage, the degree of risk also shows an increasing trend, while the frequency fluctuation shows a downward trend. This is because the fast load shedding stage fully considers the load frequency characteristics and P-V characteristics, but does not consider the risk caused by the uncertainty of the load power and the loss of load shedding. When the load shedding ratio of the first stage is set to 26%~36%, the frequency fluctuation amplitude of the system is relatively flat, the risk degree shows a slight upward trend, and the increase amplitude is low. Therefore, for the microgrid group model based on the improved IEEE33 node system, the first stage of load shedding ratio of 26% should be selected.

The microgrid group model based on the improved IEEE-118 node system is built in MATLAB/Simulink, as shown in Fig. A3. Table A3 shows the configuration information of the microgrid group, which includes three submicrogrids MG1, MG2 and MG3. The MG1 submicrogrid contains ten photovoltaic modules PV1-10, nine energy storage modules BES1-9, and twenty-six loads LD1-26. The MG2 submicrogrid contains six photovoltaic modules PV11-16, four energy storage modules BES10-13, and fifteen loads LD27-41. The MG3 submicrogrid contains four photovoltaic modules PV17-20, two energy storage modules BES14-15, and nine loads LD42-50. Table A4 shows the data information of the 50 load nodes of the system. They are classified into Level I loads, Level II loads, and Level III loads in decreasing order of level.

Table A3

Microgrid group configuration information (improved IEEE-118 node system)

Microgrid	MG1	MG2	MG3
	PV1-10	PV11-16	PV17-20
Rated photovoltaic(PV) power(kW)	7, 5, 5, 5, 5, 5, 8.5, 4, 6, 4	5, 5, 12, 12, 7, 17	5, 10, 10, 5
PV real-time power(kW)	7, 3, 3, 5, 5, 4, 8.3, 3, 5, 3	5, 5, 8, 8, 7, 7	5, 6, 6, 3
	BES1-9	BES10-13	BES14-15
Rated power of BES(kW)	6, 4, 5.5, 4, 14, 6, 10, 25, 8	13, 3, 14, 20	5, 20
BES real-time power(kW)	5, 4, 3, 3, 3, 4, 10, 20, 3	3, 3, 4, 20	3, 10

Table A4

System load data information (improved IEEE-118 node system)

Bus	Priority	$P_{LN,i}$ kW	$P_{loss,\max,Li}$ kW	$C_{loss,i}$ ($/kWh)	σ_i^2
LD1	II	5.5	2.5	1.21	0.55
LD2	I	3	1.2	2.46	0.3
LD3	III	5.5	2.1	0.56	0.55
LD4	I	4.8	1.5	3.01	0.48
LD5	II	4.1	2.1	2.27	0.41
LD6	II	17.5	11.7	1.94	1.75
LD7	II	5.6	2.8	2.31	0.56
LD8	III	2.2	1.3	0.98	0.22
LD9	III	3.1	1.7	1.84	0.31
LD10	I	6.6	2.2	2.25	0.66
LD11	III	7.1	4.3	1.05	0.71
LD12	II	4.5	2.5	2.16	0.45
LD13	I	5.3	2.1	2.71	0.53
LD14	III	2.9	1.4	1.69	0.29
LD15	III	3.6	2.2	1.26	0.36
LD16	II	4.2	2.1	2.72	0.42
LD17	III	7.8	4.2	0.97	0.78
LD18	I	5.2	2.2	2.75	0.52
LD19	III	3.7	2.1	1.03	0.37
LD20	II	1.9	0.8	2.41	0.19
LD21	III	4.8	3.2	1.42	0.48
LD22	II	8.6	5.1	1.51	0.86
LD23	I	6.3	2.8	2.63	0.63
LD24	III	5.7	3.2	0.99	0.57
LD25	III	5.5	2.5	1.2	0.55
LD26	II	3.3	1.7	1.62	0.33
LD27	II	4.9	3.1	1.41	0.49
LD28	II	3.4	2.4	1.96	0.34
LD29	III	7.8	5.8	0.56	0.78
LD30	I	7.2	3.3	2.81	0.72

LD31	I	6.3	3.1	3.07	0.63
LD32	III	5.9	3.2	1.24	0.59
LD33	II	7.2	4.6	1.58	0.72
LD34	III	9.1	7.2	0.64	0.91
LD35	III	8.6	6.6	0.71	0.86
LD36	III	5.4	4.1	1.06	0.54
LD37	II	10.5	6.5	1.55	1.05
LD38	I	9.8	4.5	2.76	0.98
LD39	III	8.3	6.8	0.87	0.83
LD40	II	7.8	4.2	1.34	0.78
LD41	II	7.9	4.0	1.22	0.79
LD42	I	5.8	2.4	3.04	0.58
LD43	II	3.9	2.1	2.54	0.39
LD44	III	3.8	2.5	1.24	0.38
LD45	II	7.6	3.3	0.79	0.76
LD46	III	4.9	2.8	1.21	0.49
LD47	II	4.5	2.1	1.36	0.45
LD48	I	5.3	2.2	2.77	0.53
LD49	III	8.6	5.6	0.81	0.86
LD50	III	15.8	10.5	0.37	1.58

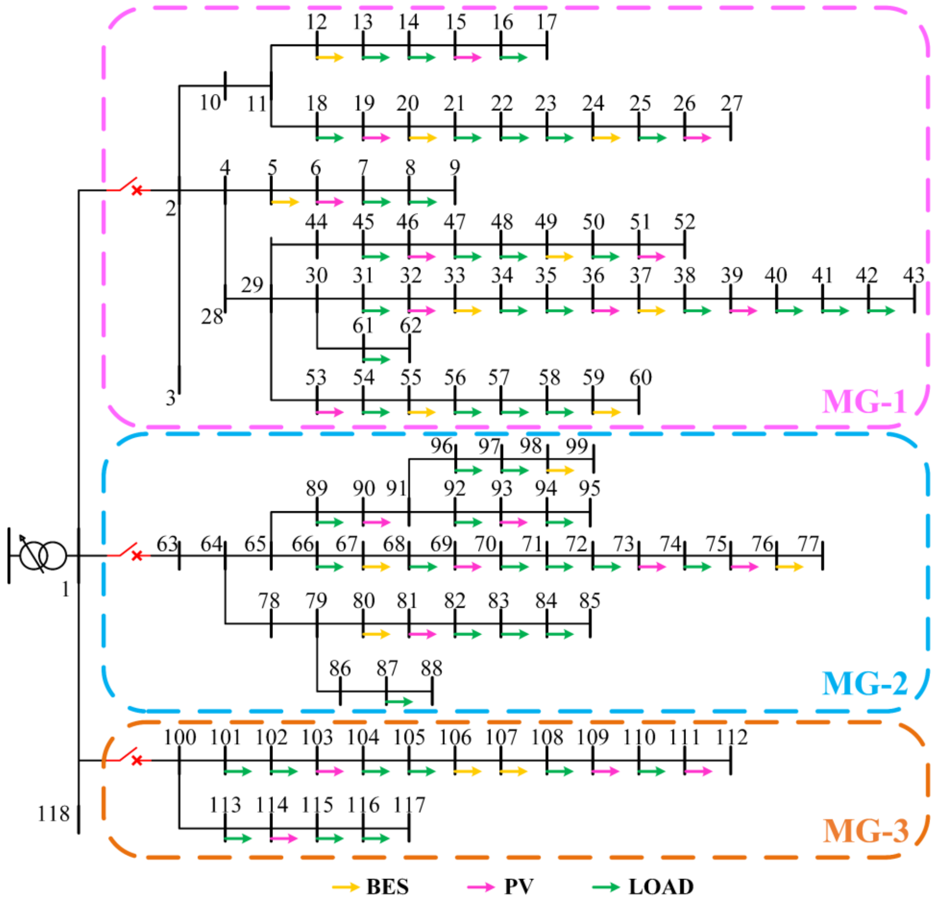

Fig. A3. Microgrid group model based on the improved IEEE-118 node system.

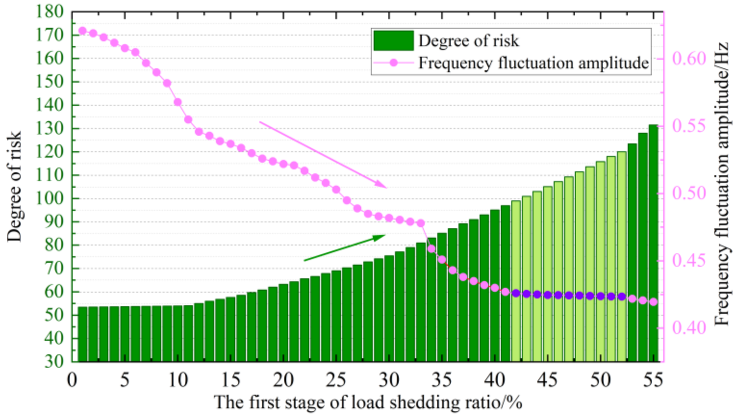

Fig. A4. Comparison chart of the risk loss degree and frequency fluctuation range under different load shedding ratios (improved IEEE-118 node system).

Table A5

Comparison of the load shedding ratio distributions in the first stage of the microgrid with different numbers of nodes

Microgrid group model	Improved IEEE-37 node system	Improved IEEE-33 node system	Improved IEEE-118 node system
The load shedding ratio range of the first stage	30%~40%	26%~36%	42%~52%
Optimal load shedding ratio of the first stage	30%	26%	42%

Fig. A4 is a comparative chart of the load risk severity indicators and frequency fluctuation amplitudes under the different load shedding ratios in the first stage (improved IEEE-118 node system). With the increase in the ratio of load shedding, the risk degree also increases, but the frequency fluctuation of the system becomes smaller. This is because the uncertainty of the load power and the loss of load shedding are not considered in the first stage of load shedding, which leads to an increase in the risk degree of the microgrid. However, the purpose of the first stage of load shedding is to prevent a rapid decrease in frequency. Therefore, the greater the ratio of load shedding in the first stage is, the smaller the frequency fluctuation of the system is. When the load shedding ratio is between 0 and 10%, the risk loss of the microgrid is low and stable, but its frequency fluctuation amplitude is large. Therefore, this interval cannot be defined as the first stage load shedding ratio. When the load shedding ratio is between 42% and 52%, the frequency fluctuation of the system is relatively stable. In this interval, the load shedding ratio corresponding to the lowest possible risk degree should be selected. Therefore, 42% was selected as the best load shedding ratio in the first stage.

Table A5 is comparison of the load shedding ratio distributions in the first stage of the microgrid with different numbers of nodes. The optimal load shedding ratios of the microgrid group model based on the improved IEEE-37 node system, the microgrid group model based on the improved IEEE-33 node system, and the microgrid group model based on the improved IEEE-118 node system are 30%, 26% and 42%, respectively. Therefore, for microgrid group models with different networks and different inertia, the ratio of load shedding in the first stage is different.

Appendix B

This section compares and analyzes the sensitivity differences of the proposed strategy in different load distribution scenarios. The normal distribution model of the active power of the node load is shown in equations (11) and (12). However, the active power of the actual node load may exhibit skewed or other irregular distribution characteristics [36]. The skew distribution model and probability density function of the load power are shown in equations (B1) and (B2):

$$P_{Li} \sim SN\left(\mu_i,\sigma_i,\lambda_i\right) \tag{B1}$$

$$\rho\left(\zeta\right)=\frac{1}{\sigma\left(\mu-a\right)\sqrt{2\pi}}\times e^{\frac{\left(\left(\frac{\zeta-a}{\mu-a}\right)^{\lambda}-1\right)^{2}\left(\zeta-a\right)^{\lambda-1}}{-2\sigma^{2}\lambda^{2}\left(\mu-a\right)^{\lambda-1}}} \tag{B2}$$

where, P_{Li} is the load active power of node i; μ_i, σ_i and λ_i are the expectation, standard deviation and skewness index of the load active power of node i, respectively. μ_i is the mean load power of node i; σ_i^2 is 10% of the expected power; and the value of λ_i is 0.5 or 1.5. The normal and skew distributions of the load active power are shown in Fig. B1.

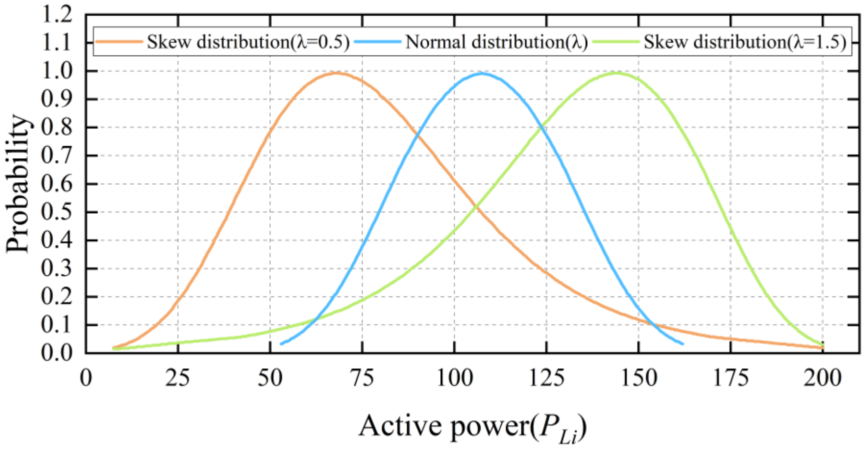

Fig. B1. The normal and skew distributions of the load active power.

Fig. B2 is the convergence curve comparison of the grasshopper optimization algorithm proposed in this paper for different distributions of the load active power. Among the three distributions, the curve obeying the normal distribution has a fast iteration speed and high solution efficiency, and the solution speeds of the positive skew (λ =0.5) and negative skew (λ =1.5) curves are slow. This is because the

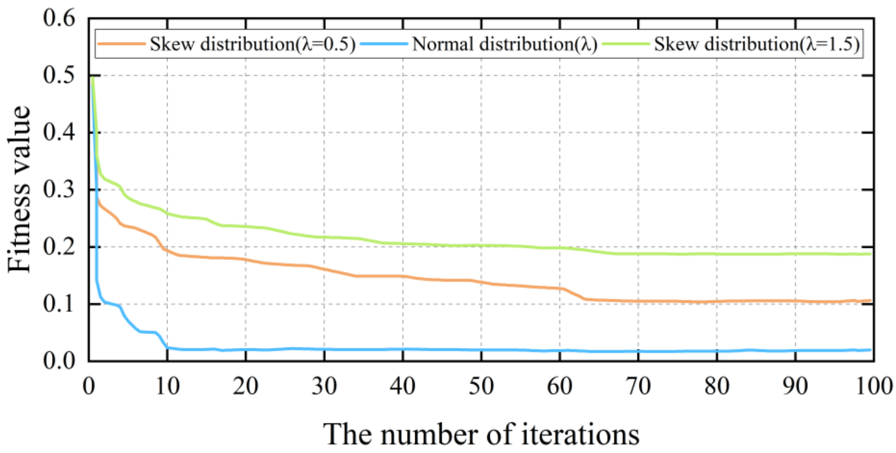

Fig. B2. Algorithm convergence comparison of three kinds of load active power distributions.

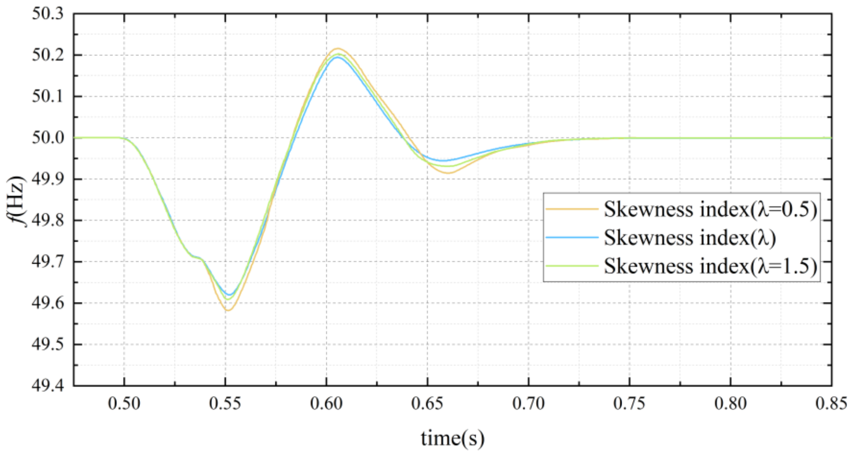

Fig. B3. System frequency recovery of normal distribution and skew distribution of the load active power.

probability density function in the case of skew distribution is more complex, which increases the complexity of the final objective function, resulting in a slower speed of final solution than that of the normal distribution curve.

Fig. B3 is system frequency recovery of normal distribution and skew distribution of the load active power. When the load active power obeys the skew distribution, the system frequency recovery effect is poor. This is because the skew distribution leads to an increase in the complexity of the load model, resulting in a slow convergence rate of the algorithm. This leads to the inability to calculate the second stage load shedding location after the completion of the first stage load shedding action, so the system frequency decreases significantly. However, the average value of the active power of the load with positive skew distribution shifts to the left, which leads to an overall decrease in the calculated load shedding and a large fluctuation in the system frequency. The negative skew distribution is opposite, and the system frequency fluctuation is small. However, the negative skew distribution curve has a large decrease in frequency due to the slow solution speed. Therefore, the final frequency fluctuation is greater than that of the normal distribution curve. Based on the above analysis, when the load active power obeys the normal distribution, the convergence speed of the algorithm and the control effect of the strategy are the best.

References

[1] Wang C, Liu C, Chen J, Zhang G. Cooperative planning of renewable energy generation and multi-timescale flexible resources in active distribution networks. Appl Energy 2024;356:122429.

[2] Xu T, Liu Z, Guo L, Meng H, Wang R, et al. Robust optimisation of electricity-heating integrated energy system based on data-driven PV interval estimation. IET Energy Syst Integr 2023;5(4):365-511. https://doi.org/10.1049/esi2.12114.

[3] Hu Z, Yao W, Shi Z, Shuai H, Gan W, Wen J. Intelligent and rapid event-based load shedding pre-determination for large-scale power systems: Knowledge-enhanced parallel branching dueling Q-network approach. Appl Energy 2023;347:121468.

[4] Liu J, Zhang Y, Meng K, Dong Z, Xu Y, Han S. Real-time emergency load shedding for power system transient stability control: A risk-averse deep learning method. Appl Energy 2022;307:118221.

[5] Chen B, Wang J, Lu X, et al. Networked Microgrids for Grid Resilience, Robustness, and Efficiency: A Review. IEEE Trans Smart Grid 2021;12(1):18-32. http://dx.doi.org/10.1109/TSG.2020.3010570.

[6] Xie C, Wang D, Lai C, Wu R, Wu X, Lai L. Optimal sizing of battery energy storage system in smart microgrid considering virtual energy storage system and high photovoltaic penetration. J Clean Prod 2021;281:125308. http://dx.doi.org/10.1109/ISC251055.2020.9239044.

[7] Zhang H, Ma S, Ding T, et al. Multi-Stage Multi-Zone Defender-Attacker-Defender Model for Optimal Resilience Strategy With Distribution Line Hardening and Energy Storage System Deployment. IEEE Trans Smart Grid 2021;12(2):1194-1205. http://dx.doi.org/10.1109/TSG.2020.3027767.

[8] Dehghanpour E, Karegar H, Kheirollahi R. Under frequency load shedding in inverter based microgrids by using droop characteristic. IEEE Trans Power Del 2021; 36(2):1097-1106. http://dx.doi.org/10.1109/TPWRD.2020.3002238.

[9] Rudez U, Mihalic R. Monitoring the first frequency derivative to improve adaptive underfrequency load-shedding schemes. IEEE Trans Power Syst 2011;26(2): 839–846. http://dx.doi.org/10.1109/TPWRS.2010.2059715.

[10] Sigrist L, Rouco L, and Echavarren F. A review of the state of the art of UFLS schemes for isolated power systems. International Journal of Electrical Power & Energy Systems 2018;99:525-539. https://doi.org/10.1016/j.ijepes.2018.01.052.

[11] Silva J, Assis T. Adaptive underfrequency load shedding in systems with renewable energy sources and storage capability. Electr Power Syst Res 2020;189:106747. https://doi.org/10.1016/j.epsr.2020.106747.

[12] Hong Q, et al. A New Load Shedding Scheme With Consideration of Distributed Energy Resources' Active Power Ramping Capability. IEEE Trans Power Syst 2022;37(1):81-93. http://dx.doi.org/10.1109/TPWRS.2021.3090268.

[13] Amraee T, Darebaghi M, Soroudi A, Keane A. Probabilistic Under Frequency Load Shedding Considering RoCoF Relays of Distributed Generators. IEEE Trans Power Syst 2018;33(4):3587-3598. http://dx.doi.org/10.1109/TPWRS.2017.2787861.

[14] Chandra A, Pradhan A. An Adaptive Underfrequency Load Shedding Scheme in the Presence of Solar Photovoltaic Plants. IEEE Syst J 2021;15(1): 1235-1244. http://dx.doi.org/10.1109/JSYST.2020.2995050.

[15] Karimi M, Wall P, Mokhlis H, Terzija V. A new centralized adaptive underfrequency load shedding controller for microgrids based on a distribution state estimator. IEEE Trans Power Delivery 2016;32:370. https://doi.org/10.1109/TPWRD.2016.2594866.
[16] Hoseinzadeh B, Silva F, Bak C. Adaptive tuning of frequency thresholds using voltage drop data in decentralized load shedding. IEEE Trans Power Syst 2015;30:2055-2062. https://doi.org/10.1109/TPWRS.2014.2351015.
[17] Rudez U, Sodin D, Mihalic R. Estimating frequency stability margin for flexible under-frequency relay operation. Electric Power Systems Research 2021;194:107116. https://doi.org/10.1016/j.epsr.2021.107116.
[18] Hosseinzadeh M, Salmasi F. Supervisory Control of a Hybrid AC/DC Micro-Grid with Load Shedding Based on the Bankruptcy Problem. Amirkabir Int J Science Res 2016. https://api.semanticscholar.org/CorpusID:36314157.
[19] Talukdar B, Sinha A, Mukhopadhyay S, Bose A. A computationally simple method for cost-efficient generation rescheduling and load shedding for congestion management. Int J Electr Power Energy Syst 2005;27.5(6):379-388. https://doi.org/10.1016/j.ijepes.2005.02.003.
[20] Hussain A, Bui V, Kim H. An Effort-Based Reward Approach for Allocating Load Shedding Amount in Networked Microgrids Using Multiagent System. IEEE Trans Ind Inform 2020;16(4):2268-2279. http://dx.doi.org/10.1109/TII.2019.2929284.
[21] Wang Z, Bian Q, Xin H, Gan D. A Distributionally Robust Co-Ordinated Reserve Scheduling Model Considering CVaR-Based Wind Power Reserve Requirements. IEEE Trans Sustain Energ 2016;7(2):625-636. http://dx.doi.org/10.1109/TSTE.2015.2498202.
[22] Asensio M, Contreras J. Stochastic Unit Commitment in Isolated Systems With Renewable Penetration Under CVaR Assessment. IEEE Trans Smart Grid 2016;7(3):1356-1367. http://dx.doi.org/10.1109/TSG.2015.2469134.
[23] Skrjanc T, Mihalic R, and Rudez U. A systematic literature review on underfrequency load shedding protection using clustering methods. Renewable and Sustainable Energy Reviews 2023;180:113294. https://doi.org/10.1016/j.rser.2023.113294.
[24] Hong Y, Wei S. Multiobjective underfrequency load shedding in an autonomous system using hierarchical genetic algorithms. IEEE Trans Power Del 2010;25(3):1355-1362. http://dx.doi.org/10.1109/TPWRD.2010.2046679.
[25] Hong Y, Hssiao M, Chang Y, et al. Multiscenario underfrequency load shedding in a microgrid consisting of intermittent renewables. IEEE Trans Power Del 2013;28(3):1610-1617. https://doi.org/10.1109/TPWRD.2013.2254502.
[26] Jallad J, Mekhilef S, Laghari J, Mokhlis H. Improved UFLS with consideration of power deficit during shedding process and flexible load selection. IET Renew Power Gener 2018;12(5):565-575. https://doi.org/10.1049/iet-rpg.2017.0170.
[27] Musyoka P, Musau P, Nyete A. Optimal load shedding scheme for a model renewable energy micro-grid. 2020 IEEE power energy soc. Ind. Appl. Soc. PowerAfrica. Nairobi, Kenya: IEEE; 2020. p. 1–5. https://doi.org/10.1109/PowerAfrica49420.2020.9219902.
[28] Wang C, Chu S, Yu H, Ying Y, Chen R. Control strategy of unintentional islanding transition with high adaptability for three/single-phase hybrid multimicrogrids. Int J Electr Power Energy Syst 2020;136:107724. https://doi.org/10.1016/j.ijepes.2021.107724.
[29] Hussain A, Bui V, Kim H. An Effort-Based Reward Approach for Allocating Load Shedding Amount in Networked Microgrids Using Multiagent System. IEEE Trans Ind Inform 2020;16(4):2268-2279. http://dx.doi.org/10.1109/TII.2019.2929284.
[30] Huang Q, Huang R, Hao W, Tan J, Fan R, Huang Z. Adaptive power system emergency control using deep reinforcement learning. IEEE Trans Smart Grid 2020;11(2):1171–1182. https://doi.org/10.1109/TSG.2019.2933191.

[31] Tang J, Liu J, Ponci F, Monti A. Adaptive load shedding based on combined frequency and voltage stability assessment using synchrophasor measurements. IEEE Trans Power Syst 2013;28(2): 2035–2047. http://dx.doi.org/10.1109/TPWRS.2013.2241794.
[32] Cao Y, Wei W, Mei S, Shafie-khah M, Catalão J. Analyzing and Quantifying the Intrinsic Distributional Robustness of CVaR Reformulation for Chance-Constrained Stochastic Programs. IEEE Trans Power Syst 2020;35(6): 4908-4911. http://dx.doi.org/10.1109/TPWRS.2020.3021285.
[33] Roveto M, Mieth R, Dvorkin Y. Co-Optimization of VaR and CVaR for Data-Driven Stochastic Demand Response Auction. IEEE Contr Syst Lett 2020;4(4):940-945. http://dx.doi.org/10.1109/LCSYS.2020.2997259.
[34] Esfanhani M, Hariri A, and Mohammed O. A multiagent- based game-theoretic and optimization approach for market operation of multimicrogrid systems. IEEE Trans. Ind. Inform 2019;15(1):280–292. http://dx.doi.org/10.1109/TII.2018.2808183.
[35] Jia L, Zhu Y, Du S, Wang Y. Analysis of the transition between multiple operational modes for hybrid AC/DC microgrids. CSEE J Power Energy Syst 2018;4(1):49-57. http://dx.doi.org/10.17775/CSEEJPES.2016.01030.35.
[36] Zhang Y, Wen H, Wu Q and Ai Q. Optimal Adaptive Prediction Intervals for Electricity Load Forecasting in Distribution Systems via Reinforcement Learning. IEEE Trans Smart Grid 2023;14(4):3259-3270. http://dx.doi.org/10.1109/TSG.2022.3226423.